Thermomechanical stress analysis of superplastic forming tool

Cy Gao, Philippe Lours, Gérard Bernhart

HAL Id: hal-01716113
https://hal.science/hal-01716113

Submitted on 11 Jan 2019

Thermomechanical stress analysis of superplastic forming tools

C.Y. Gao, P. Lours, G. Bernhart *

Ecole des Mines d'Albi-Carmaux, Reseach Center on Tools, Materials and Processes (CROMeP), 81013 Albi CT Cedex 09, France

Abstract

A thermomechanical stress analysis of a superplastic forming (SPF) tool is performed by means of the finite element simulation of the whole forming process. The distributions of residual stress and distortion within the tool are investigated in order to evaluate the damage effects of thermomechanical loading. The effect of cyclic loading is related to the fact that residual stress and distortion in the tool accumulate as loading cycles proceed. The characteristics of the typical forming parameters of the sheet are described too. Meanwhile, the numerical simulation can be employed to compare various materials that can be used to manufacture forming tools.

Keywords: Superplastic forming process; Forming tools; Finite element simulation; Thermomechanical analysis

1. Introduction

The superplastic forming process is one of the most advanced manufacturing methods for producing highly complex thin-sheet components in a single operation. This process is widely used in aerospace industry. Superplastic forming (SPF) shows significant advantages as compared to conventional forming methods. Superplastic metals exhibit high ductility and very low resistance to deformation and are particularly suitable for forming processes that require very large deformation. Superplastic forming is usually completed within only one step and intermediate annealing is usually not necessary. This process allows the production of complex, deep-shaped parts with quite uniform thickness. Drawbacks of the process include the need of tight control of temperature and strain rate. Very long forming time makes this process impractical for high volume production series. In addition, the high cost of Ti–6Al–4V sheet metal [1] is a limiting factor for wide and generalized spreading of the technology. So, the majority of SPF production still remains in the aerospace, transport and architectural fields.

A typical cycle of superplastic forming process consists in the following sequences:

(I) the mould is heated up to the required temperature in the heating press, typically up to 900 °C for Ti–6Al–4V alloy;

(II) clamping pressure is applied on the boundary of sheet so as to clamp it with the mould whose surface forms a cavity of the required shape;

(III) gas pressure is applied to the opposite surface of the sheet, forcing it to gradually acquire the exact inner shape of the mould;

(IV) the mould is pulled out from the heating press for removing the formed component, and then pushed into the heating press again with a new sheet for forming a new component;

(V) the process from II to IV is repeated as many times as necessary to produce the required amount of components to be manufactured in one forming campaign;

(VI) after forming work, the mould is taken out and exposed to ambient air so that the temperature decreases gradually down to room temperature. The latter step is sometimes performed in the heating press to avoid any thermal shock.

A number of theoretical and numerical analyses have been performed for modeling superplastic forming. The contribution of numerical simulation is demonstrated clearly because industrial cases are very different from each other and require

a particular attention [2]. Finite element simulation has been used extensively in the last few years to model SPF processes [3]. It has been shown to be a viable approach to model non-linear material behavior and contact friction phenomena, and it is beneficial to predict the deformation behavior especially for complex shapes. However, researches in the past mainly focused on the development of new advanced superplastic materials more than on the optimization of the technological aspects of the process, like the reduction of the forming time or the design of low cost forming tools. In particular, there has not been enough research on superplastic forming tools because they are generally considered as rigid body. Unfortunately, the current industrial growth of SPF for titanium alloy forming has been limited by the quality and durability problems of tools [4].

Tools are fundamental for the success of most manufacturing processes including superplastic forming processes. Satisfactory tools should be [5]: (i) accurate, able to continuously produce components at required dimensions and surface quality; (ii) durable, able to continuously operate at elevated temperature with no damage and to safely contain the gas pressure and the applied mechanical forces; (iii) productive, able to produce the highest output while controlling the pressure loading cycle to keep the maximum strain rate near the optimum value through the whole forming process and (iv) economical, able to manufacture components at minimum cost for optimized forming conditions.

Tool damage can be mainly attributed to one of the following causes [6]: type and quality of tool steels, design and manufacturing of the mould, surface treatment and heat treatment and effects of the forming process. In the case of SPF, the last factor includes three aspects:

(a) Permanent distortion: heating and cooling of tools will generate temperature gradients and thermal stress in tools. The thermal stress as well as the mechanical stress can result in creep deformation of the tools, leading to a lost of dimension and accuracy in the formed components. Furthermore, long-termed exposure at high temperature in aggressive environment may induce micro-structural changes in materials, which also result in detrimental evolution of the dimensions of tools [7].
(b) Cracking: initial micro-cracks can be caused by thermomechanical loading and cycling operation of tools. Macro-cracks will appear first in regions with high stress concentration [8]. This will be developed further in Section 2.2.
(c) Oxidation and oxide spallation: these phenomena can impair the surface of the mould, and thus alter the surface quality of the formed components [9,10].

In this paper, we have considered the superplastic forming of an axisymmetric box. The numerical simulation of the mould and sheet is performed thermomechanically for the whole superplastic forming process. The distribution of residual stress and deformation of the mould are investigated in order to analyze the damage effects of the thermomechan-ical loading on the mould. The finality of the research is to enhance the quality of tools and increase their service lifetime.

2. Materials and finite element modeling

2.1. Presentation of materials

Selection of tool materials includes consideration on both the mechanical properties and the oxidation resistance. Ni–Cr–Fe high-alloyed heat resistant cast steels are commonly used to manufacture superplastic forming tools for titanium alloys sheets. Other materials, such as reinforced concretes or ceramics, are still under investigation [11]. Heat resistant cast steels, either austenitic or ferritic, show satisfactory performance as their high chromium content ensures a good resistance to oxidation damage, and the addition of nickel and carbide elements provides rather high strength at high temperature. Table 1 shows the chemical composition of the superplastic tool material investigated in the paper.

The density of the material is 8200 kg/m^3 and the Poisson ratio is 0.29. Other related parameters vary with temperature as indicated in Fig. 1 where the experimental data are plotted. The units of these parameters are as follows: Young's modulus E is MPa; thermal expansion ε is 1/K; thermal conductivity k is J/(m s K) and specific heat c_p is J/(kg K).

Rate-dependent plasticity is the constitutive relation of the mould and the sheet. The power-law creep model is attractive for its simplicity. It is defined by the equivalent uniaxial behavior for modeling steady state creep. As the stress state remains essentially constant, the time-hardening form is used here:

$$\dot{\bar{\varepsilon}}_{eq}^{cr} = A\tilde{\sigma}^n t^m \tag{1}$$

where $\dot{\bar{\varepsilon}}_{eq}^{cr}$ is the uniaxial equivalent creep strain rate; $\sqrt{\frac{2}{3}\dot{\varepsilon}^{cr} : \dot{\varepsilon}^{cr}}$; $\tilde{\sigma}$ the uniaxial equivalent deviatoric stress (for isotropic case, it is Mises equivalent stress); t the total time (in second) and A, n, m are the constant parameters that are functions of temperature.

For physically reasonable behavior, A and n must be positive and $-1 < m \leq 0$. Their values are listed in Table 2. Obviously, the creep law varies with temperature because

Table 1
Chemical composition of the tools investigated (wt%)

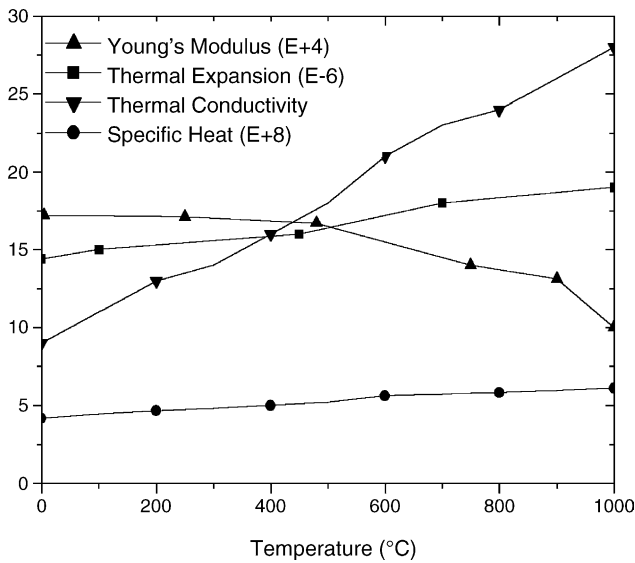| Material name	GX45NiCr49_27
Fe	Balance
C	0.458
Si	1.21
Mn	0.98
S	0.001
P	0.008
Ni	49
Cr	26.76
W	4.95

Fig. 1. Temperature depending parameters of materials GX45NiCr49_27.

Table 2
Creep-law parameters of sheet and mould

Materials	A	n	m
Mould (GX45NiCr49_27)	6.0052E−12	3.8493	−0.4769
Sheet (Ti–6Al–4V)	2.27341E−06	1.7540	0

all the parameters are function of temperature. Since the total time is used in the expression, such reasonable behavior also typically requires that small time steps, compared to the creep time, be used for any steps in which creep is not operative.

In practice, the experimental data of strain versus time are measured under different stress values at a given temperature [12]. The experimental data at 900 °C are shown in Fig. 2 and the fitting curves are obtained using allometric power
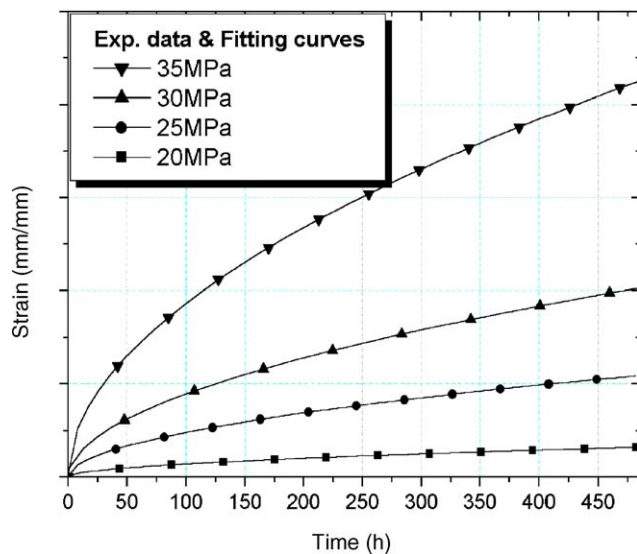

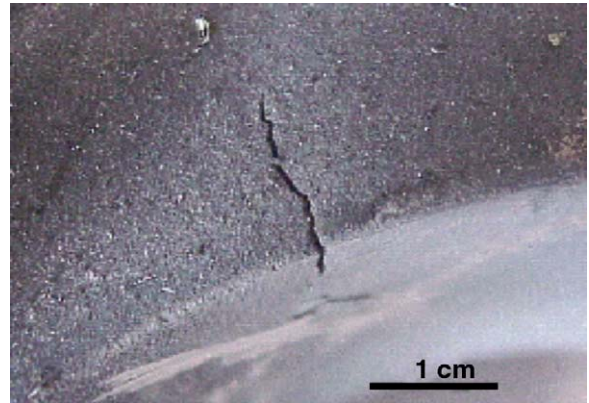Fig. 2. Relation of strain vs. time under different stress values at 900 °C.

Fig. 3. Example of tool damage after cumulative SPF cycles.

function. On the basis of these curves, the parameter of the creep law of the material at 900 °C is derived.

The material of sheet is chosen as Ti–6Al–4V. The material is isotropic; its Poisson ratio is 0.29 and Young's modulus is 1.0 GPa corresponding to the temperature 950 °C. The parameters [13] of the "time-hardening" constitutive equation are listed in Table 2.

In addition, the sheet's target strain rate during forming is 3.0×10^{-4} s. It can be adjusted for different forming process.

2.2. Tool damage

The thermomechanical stresses generated by the SPF process, result in dies damages which generally initiate on geometrical imperfections that can be either internal to the die, such as foundry defects or external to the die, for instance, surface defects (machining grooves, oxide inclusion or oxide spall). Cracks can also propagate from zones, imperfectly designed and drawn, where high salient angle concentrates stresses (Fig. 3). Damage due to cumulative thermal cycles proceeds via the propagation of cracks within the material according to specific routes, namely along the eutectic carbides, located within the interdendritic spaces of the heat resistant cast steel. A thorough analysis of fracture surface using scanning electron microscopy indicates unambiguously that the initiation and the propagation of cracks are due to fatigue consistently with the SPF loading conditions.

2.3. Finite element modeling

The finite element models are implemented in computer aided design software I-DEAS®, and can be transfer to another finite element software Abaqus® in the translated compatible form. The calculations are then performed in Standard Abaqus®.

The axisymmetric example is selected in order to reduce the computational time and costs. The geometric model is illustrated in Fig. 4.

Because it is an axisymmetric model, only half of the axial cross section needs to be plotted in the X–Y plane. As shown
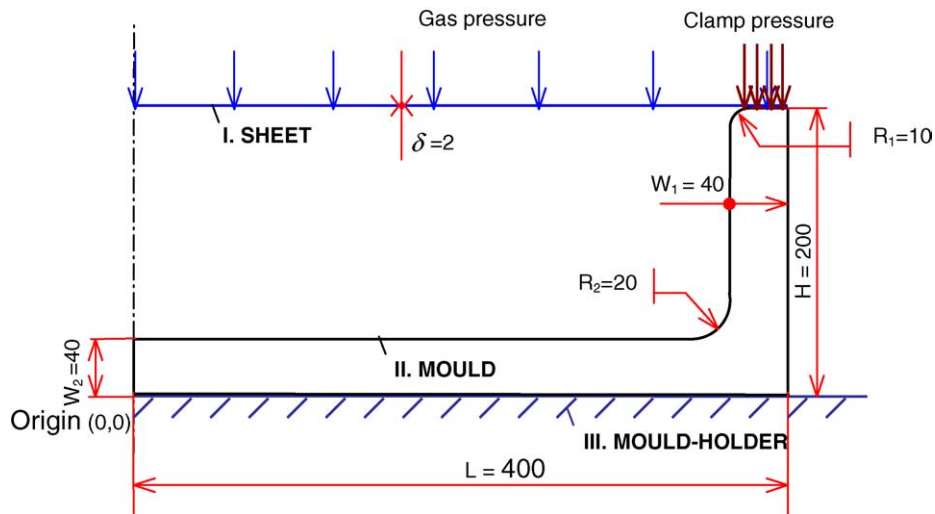
Fig. 4. Geometric model of the axisymmetric example (length unit: mm).

in Fig. 4, there are three parts in the whole model: the sheet, the mould and the mould-holder. The argon gas pressure is applied on the sheet to form it to the required component. The clamping pressure is applied on the boundary of the sheet so as to fix it with the mould during the forming process.

The finite element model is just established on the geometric model. The meshing of the sheet is generated using axisymmetric membrane element MAX1. The element size is 2 mm. The meshing of the mould-holder is generated using axisymmetric rigid element RAX2. This means that the mould-holder is considered as a rigid body and is modeled only as a rigid surface. The meshing of the mould is shown in Fig. 5. The axisymmetric four-node bilinear solid element CAX4 is chosen. The element size on the sheet-mould con-

tact surface is 3 mm so as to be compatible with the size of the sheet. It is better to have a good match of the element sizes of the bodies in contact.

Mapping meshing is taken as the meshing method for the mould to differentiate the element sizes between the surfaces and the inner regions. Because the thermal gradients decrease from the surfaces to the inner regions gradually, meshing should be finer at the surface than at the inner region. It is the finest in the vicinity of the inner fillet (curvature radius is 20 mm) and top surface where the clamping pressure is applied.

There are 4438 nodes and 4157 elements all together. In Fig. 5, three nodes on the inner contact surface, N2281, N3540 and N4185, are selected as critical points to be used in the result graphs.
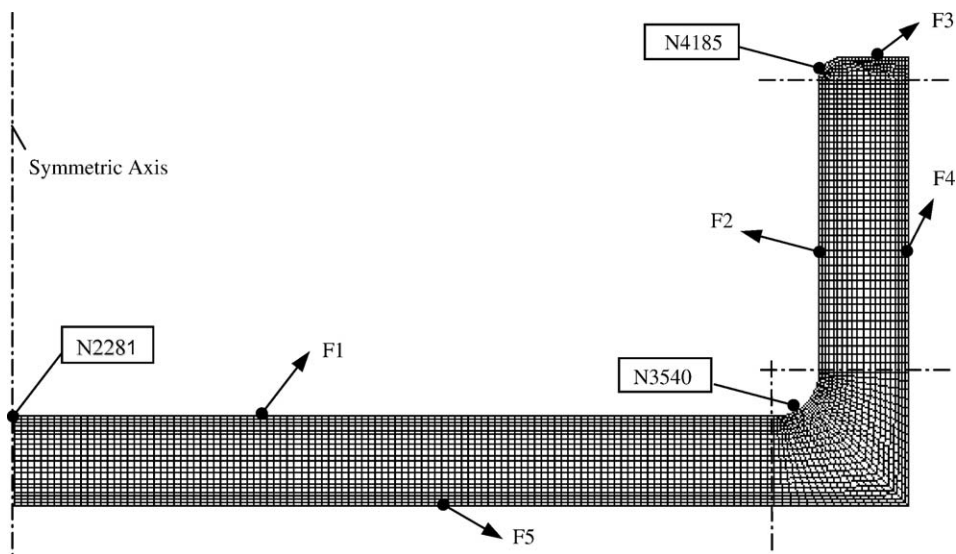

Fig. 5. Meshing of axisymmetric mould.

In any case, it is important to define correct boundary conditions for the FE model. For example, the rigid body must have a reference point totally fixed in each component. The sheet is fixed with the mould by constraining its outer-end node with the nearest node of mould by the use of node constraint equations. The surface temperatures are specified as boundary conditions usually. The inner surfaces, including F1, F2 and F3, are 850 °C, the bottom surface F5 is 900 °C and the outer side surface F4 is let to be free (see Fig. 5).

The gravity of the mould has been considered and used to prevent from the axial rigid-body motion of the mould. Of course, it should be applied before all the other loadings. In addition, the flat initial configuration of the membrane model for the sheet is entirely singular in the normal direction unless it is stressed in biaxial tension. A small biaxial initial stress has been applied to prevent this problem by defining initial stress conditions.

3. Numerical simulation

3.1. Presentation of steps

One cycle of forming process includes different periods. The calculation is divided into several computational steps according to the loading types of the whole forming process:

Step I. Tool heating period: the temperature field is introduced into the mould and results in thermal deformation and thermal stress. There are certain thermal gradients in the mould due to the non-isothermal boundary conditions on the inner and bottom surfaces of the mould. In general, the gradient can be as high as 50 °C [8]. The sequentially coupled thermal stress analysis is applied here, by using an uncoupled steady state heat transfer analysis first, and then a thermal stress analysis.

Step II. Sheet forming period: the superplastic forming process of the sheets is fulfilled in the mould by applying both the forming and the clamping pressures. The determination of the forming parameters, such as the pressure loading cycle and the final thickness distribution, is essential not only for reducing the forming time but also for achieving successful forming of complex parts. Different friction cases of the sheet-mould contact interaction are investigated, respectively, and compared with each other. During this step a viscous analysis is performed.

Step III. Mechanical unloading period: the forming and clamping pressures are released simultaneously and instantly.

Step IV. Tool cooling period: the mould's temperature decreases naturally to room temperature. The static thermal stress analysis is adopted, as creep is not taken into account at low temperatures.

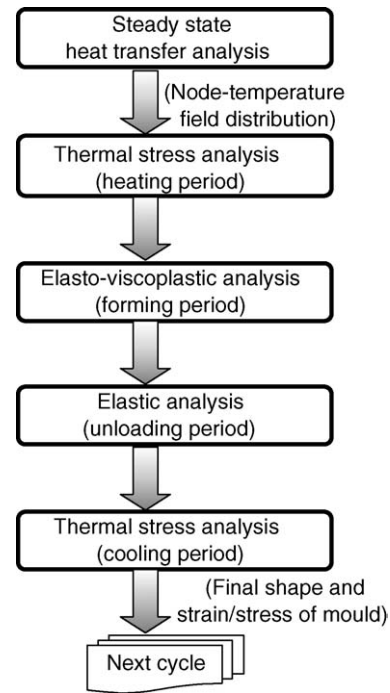The flowchart of the Abaqus calculation program is shown in Fig. 6.

Fig. 6. Flowchart of Abaqus calculation program.

3.2. Loading and controls

3.2.1. Forming load

Superplastic materials exhibit very high tensile elongation, typically 500% or more, in a particular range of temperature and strain rate. Such superplasticity in a material depends highly on the strain rate and occurs only within very tight tolerance of strain rate. There is an optimum value that is material dependent (usually very low, such as 10^{-3} to 10^{-5} s) [14]. Therefore, it is crucial to determine the pressure loading cycle before the actual forming so as to maintain the maximum strain rate near the optimum value throughout the whole forming process.

In Abaqus algorithm, parameter RATIO is calculated during each increment. It is defined as:

$$\text{RATIO} = \left. \frac{\dot{\bar{\varepsilon}}^{cr}_{eq}}{\dot{\varepsilon}^{cr}_{target}} \right|_{max} \tag{2}$$

It means the maximum value of the ratio of the equivalent creep strain rate $\dot{\bar{\varepsilon}}^{cr}_{eq}$ to the target creep strain rate $\dot{\varepsilon}^{cr}_{target}$ for any integration point in a specified element set. Here, the target creep strain rate is just the optimum creep strain rate, which is characteristic of the selected sheet material. The equivalent creep strain rate is defined by Eq. (1).

3.2.2. Clamping load

The forming process requires that the clamping load ($F_{clamping}$) applied on the top surface of the mould is kept constant. It is closely related to the level of forming pressure and can be specified according to the practical requirement

as,

$$F_{\text{clamping}} = \text{const} = 0.5\,\text{MPa} \times S_{\text{for min } g} \tag{3}$$

Thus

$$p_{\text{clamping}} = \frac{F_{\text{clamping}}}{S_{\text{clamping}}} = \frac{S_{\text{for min } g}}{S_{\text{clamping}}} \times 0.5\,\text{MPa} \tag{4}$$

where F is the load, S the area and p is the pressure. The clamping pressure is 2.8 MPa for this example. In addition, the total loading applied on the mould is known as:

$$F_{\text{mould}} = F_{\text{for min } g} + F_{\text{clamping}} \tag{5}$$

It actually varies during the sheet forming process due to the automatic adjustment of the forming pressure.

3.2.3. Contact controls

There are two contact types in our simulation. One takes place between the sheet and the mould and belongs to deformable-to-deformable type; the other lies between the mould and the mould-holder and belongs to deformable-to-rigid type. To force the calculation to converge successfully, the contact problems must be dealt carefully. Several important features are described in the following.

It is critical to define the master surface and the slave surface correctly for a contact pair at the beginning. Rigid surfaces should act as the master surface and the slave surface should be attached to deformable bodies. For two deformable surfaces, the master surface should be chosen from the surfaces of the stiffer body or the surfaces with the coarser mesh. In the forming process, the mould is always chosen as the master surface of the sheet-mould contact pair. Furthermore, the master surface should be element-based and the slave surface should be node-based. The meshes of the two surfaces should match perfectly, or be finer for the slave surface than for the master surface. However, it is permitted for the master surface nodes to penetrate the slave surface in the Abaqus master–slave contact algorithm, but not vice versa.

Contact along the perimeter of the master surface should be avoided. Otherwise, the slave surface nodes can fall off the free edge of the master surface and may be approach the mating master surface from behind. So, it is necessary to extend the master surface far enough in the finite-sliding contact models.

All the constraints of the model need to be checked to avoid the overstraining problem. At the same time, insufficient constraints should be avoided too. Because rigid body motion will occur when a body is not sufficiently restrained.

4. Results and discussion

4.1. Output related to sheet

The forming process is achieved completely after 2917 s. In Fig. 7, the evolution of the forming pressure is plotted
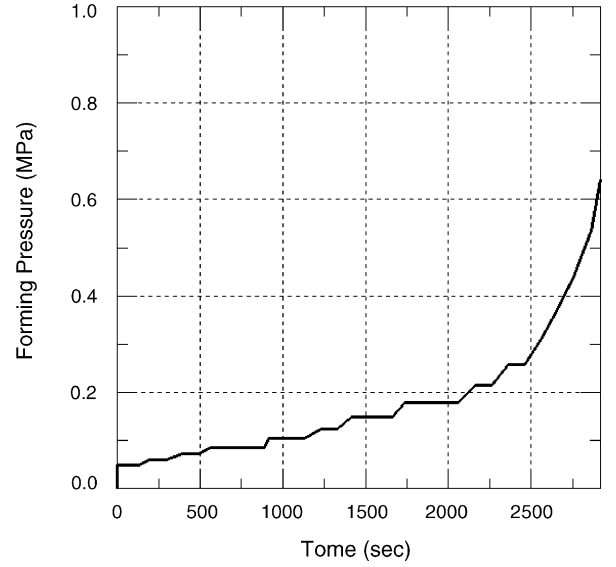

Fig. 7. Forming pressure vs. forming time.

versus time. The initial pressure is 0.1 MPa, and increases gradually up to 0.65 MPa. The highest forming pressure is required at the end of the forming process in order to satisfactorily shape the corner of the sheet.

The sheet's displacements in axial direction at different times are shown in Fig. 8 to reveal the sheet's deformation shape during the forming process. The time interval is selected as 600 s or so.

The shape at the beginning results from the application of the initial stress conditions. It is clear that the inner fillet finally needs more time as well as more pressure to acquire its curving shape. So, the radius of the fillet should not be too small so as to reduce forming cost.

In sheet forming process, one of the most critical problems is the proportional distribution of the thickness at the end of
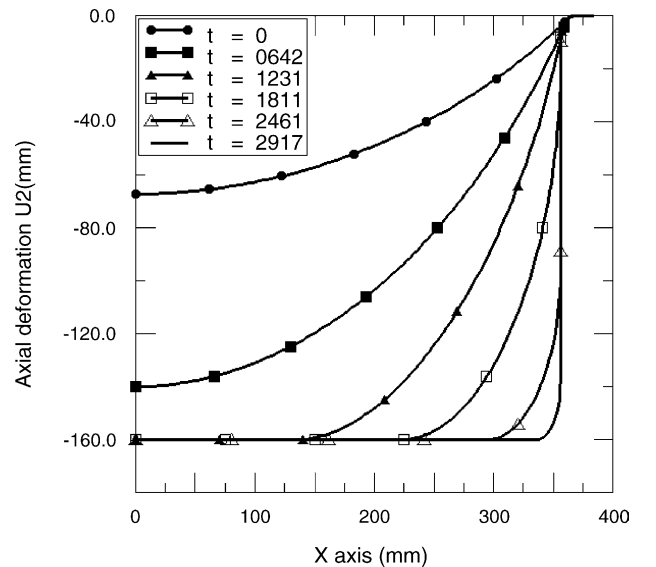

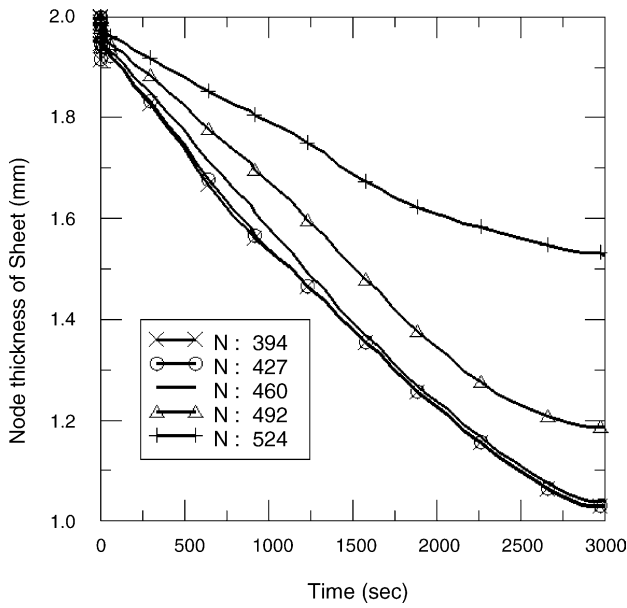Fig. 8. Shape of sheet during the forming process.

Fig. 9. Thickness evolution of the sheet at critical nodes.

Table 3
Comparison of forming parameters for different contact frictions

Parameters	No friction	$f=0.2$	$f=0.5$
Min thickness (mm)	1.03	0.94	0.94
Max Mises stress of mould (MPa)	6.93	14.45	38.09
Max contact force (N)	1.186E5	1.354E4	3.844E4
Max forming pressure (MPa)	0.65	1.30	3.75
Total forming time (s)	2917	3350	3500
Computing time (s)[a]	498	602	609

[a] The wall-clock time in the SUN workstation (Ultra SPARC-II 360 MHz) with 256 MB memory installed.

the process. The thickness evolution of the sheet at several critical nodes is shown in Fig. 9. The node number of the sheet increases from N394 to N524. Here, N394 is the inner central node and N524 is the outer-end node.

The initial thickness of the sheet is 2 mm. The final minimum thickness is almost half of the initial thickness.

Forming parameters under different contact frictions are compared in Table 3 to present the significant effect of the friction on the forming process. Further information about numerical treatment of contact and friction can be seen in Ref. [15].

The minimum thickness is achieved at the inner fillet. The maximum stress in the sheet lies around the upper fillet of the mould. The position of maximum contact pressure varies with the friction coefficient. It lies at the inner fillet when there is no friction, at the middle of the wall when friction is 0.2 and at the upper fillet when friction is 0.5. From the data in the table, it can be concluded that the forming cost would be lower if less friction is generated on the contact surface.

Moreover, an increase of friction from 0 to 0.2 doubles the required forming pressure and the maximum Mises stress in the mould. This confirms the importance of the diffusion barrier commonly referred to as "stop off" which are usually used in industry to decrease friction and avoid detrimental interaction between the sheet and the die.

4.2. Output related to the mould

4.2.1. Heating phase

As the initial temperature field of the mould does not depend on the stress field, its distribution is generated by a pure steady state heat transfer analysis. Nodal temperatures are stored as a function of time in the binary results file by specifying output variable NT in the node file option. And then, the node temperature file is introduced into the mechanical analysis program as initial conditions. The node temperature decreases from the bottom surface to the inner surface. The maximum temperature gradient between them is 50 °C.

The mould's shape after the heating phase has been checked. Compared with the original configuration, the outer part of the mould extends 6.5 mm in radial direction due to the thermal expansion, and ascends a little in axial direction due to the temperature gradient. The mould is distorted and looses contact with the substrate.
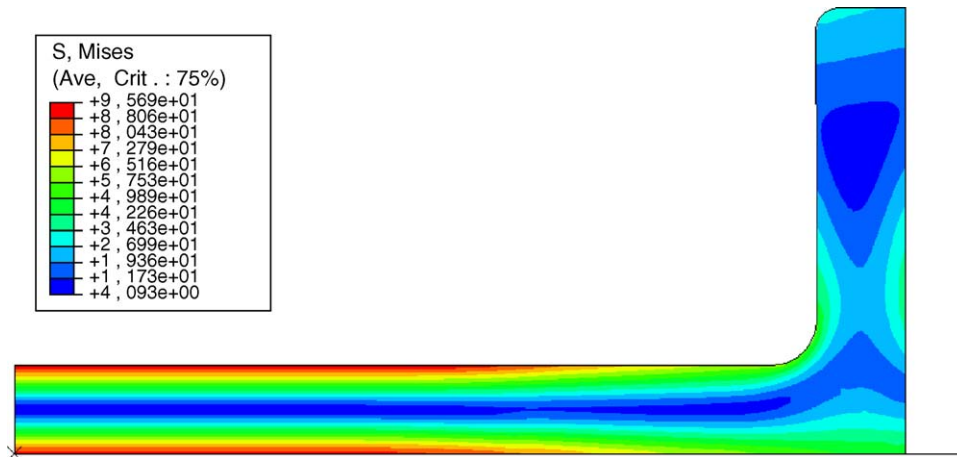

Fig. 10. Stress distribution after clamping corresponding to elastic period.

4.2.2. Clamping phase

Before forming, the clamping load is applied in order to ensure tightness of the mould prior to argon gas introduction. It brings the mould in contact with the substrate and introduces high stresses in the mould. Von Mises stresses after clamping corresponding to an elastic calculation are shown in Fig. 10. The highest stresses (almost 100 MPa) are reached in the base surfaces of the mould (tensile at the top and compressive at the bottom).

This values have to be compared to the true elastic limit of the material at 900 °C, namely around 50 MPa [16], temperature at which refractory steel behavior can be considered as nearly perfect plastic materials.

4.2.3. Sheet forming phase

After applying the clamping load and forming pressure on the mould, high temperature creep appears in the mould. The stress is relaxed dramatically due to the creep phenomenon.

(a)

Radial stress

(b)

Mises stress
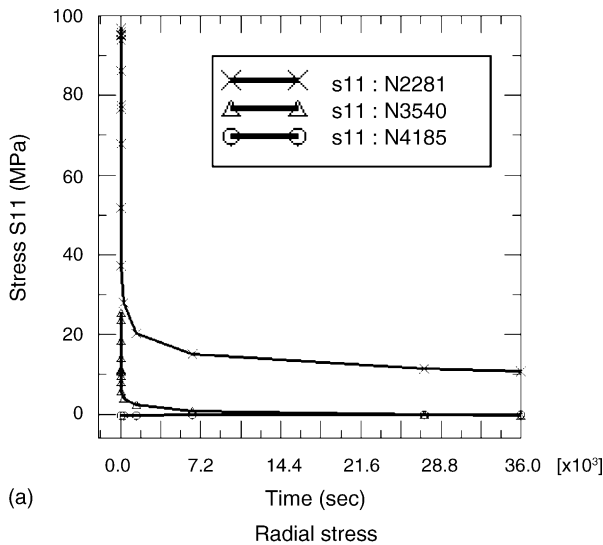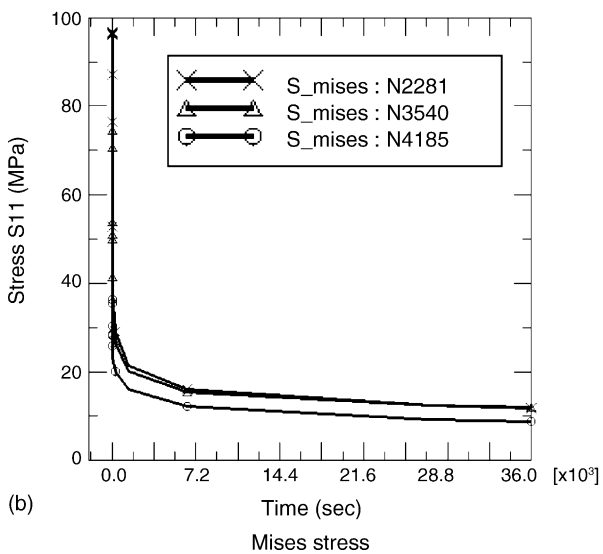
Fig. 11. Stress relaxation at critical nodes during the forming period.

Histories of stress relaxation for critical nodes are given in Fig. 11a and b, where a long forming time of 10 h was simulated. It can be seen that most of the stress relaxation is reached only within 600 s.

The total strain is composed of different parts:

$$\varepsilon_{\text{total}} = \varepsilon_{\text{mech}} + \varepsilon_{\text{thermal}} = \varepsilon_{\text{elast}} + \varepsilon_{\text{inelast}} + \varepsilon_{\text{thermal}} \qquad (6)$$

The inelastic strain $\varepsilon_{\text{inelstic}}$ in this example is just the creep strain, given in Fig. 12a and b to show the level of plastic deformation. However, the thermal strain $\varepsilon_{\text{thermal}}$ is the major one in the total strain, and results in the main deformation of the mould. The difference of thermal strain between the inner surface and the bottom surface is about 0.1%, which is the critical reason of mould's distortion. A better control of this thermal gradient during forming process would be an effective way to reduce mould distortion.

In the previous results, stresses induced in the mould by the sheet forming pressure and the clamping pressures were investigated in the combined state. Such combined simulation becomes very costly for complex 3D tools. In order to determine the major factor of damaging stresses, the stress distribution resulting from the forming and clamping pressures has been investigated separately before any creep relaxation in the mould.

Forming stress is shown in Fig. 13, and the stress distribution after clamping has been given in Fig. 10. It is obvious that stress concentration regions and stress levels are rather different for them. For the forming pressure, the stress concentration region lies in the upper part of the mould with a low level of 10 MPa, while the concentrated clamping stress is close to 100 MPa in the base of the mould. Furthermore, the damaging stress mainly lies in the base of the mould, and the forming stress is much lower there. As a consequence, if our primary interest of simulation is the stresses and distortion in the mould, the simulation of sheet forming could be omitted.

4.2.4. Thermomechanical unloading phase

After unclamping and cooling, the final shape of the mould shown in Fig. 14 indicates some changes relative to the original configuration. The deformation is magnified 30 times for better visibility.

The maximum displacement in the x direction is 0.036 mm located at the top of the mould and the maximum displacement in the y direction is 0.39 mm located at the center of the mould. Obviously, the axial distortion at the center of the mould is much higher than the radial distortion.

The residual stress at critical nodes after the unloading period is given in Fig. 15a and b. The period from 36,002 to 36,003 s corresponds to the mechanical unloading, i.e. the period where the clamping and the forming loads are both released. The period from 36,003 to 36,004 s corresponds to the cooling process, i.e. the period required to reach room temperature uniformly within the entire the mould. Only elastic calculations were performed assuming that no creep occurs at low temperatures.
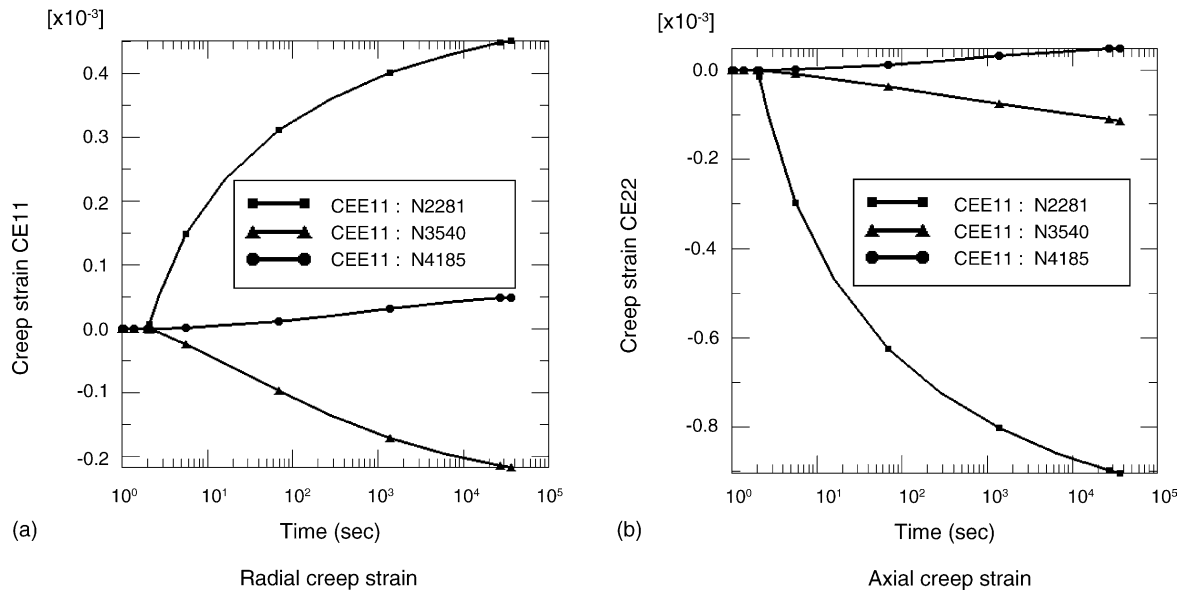
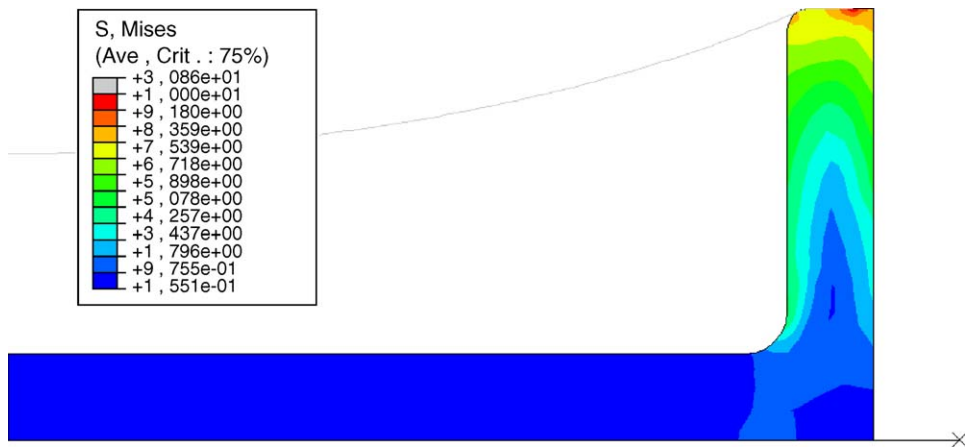Fig. 12. Creep strain history at critical nodes during forming period.

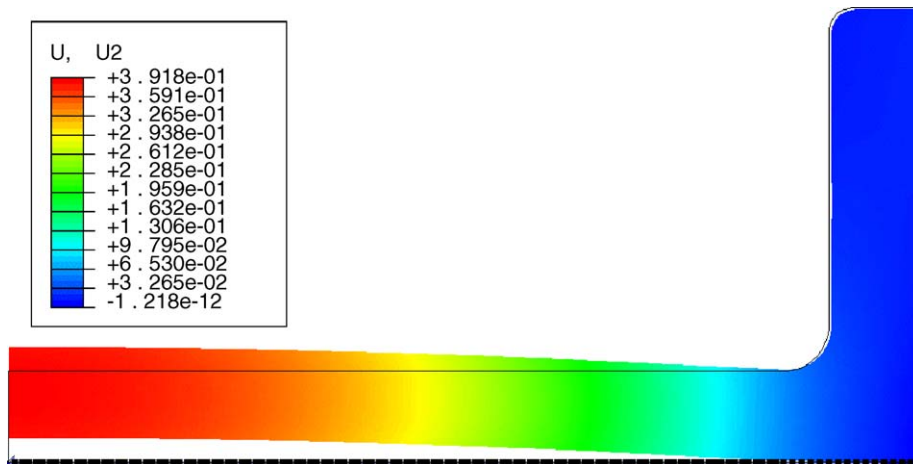Fig. 13. Forming stress corresponding to elastic period.

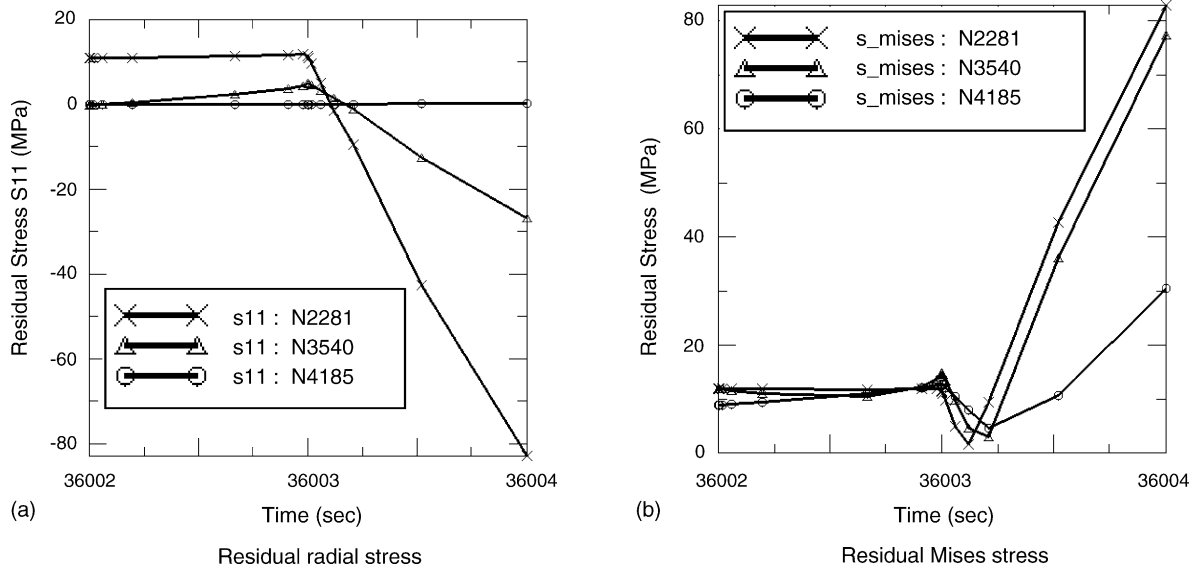Fig. 14. Deformation of the mould after the unloading period.

Fig. 15. Residual stress at critical nodes after the unloading period.

On the inner surface of the mould, lies the concentrated region of residual stress, and in fact, the residual Mises stresses at node 2281 and 3540 are almost the highest values. Because the maximum Mises stress during the whole process is only equal to 74.0 MPa, the residual stresses are really noticeable in the analysis of damage effects on the mould. In this case, the most damaging effect is the geometrical distortion of the mould.

4.2.5. Effect of forming time on the mould

Some mechanical results after one loading cycle corresponding to different forming times are listed in Table 4.

The case of 10 h is used in the calculation. It means that, just like the actual case, almost 10 components are formed in one production campaign. It is obvious that if the quantity of produced parts is increased, then the residual displacement and stress will be higher; and as a consequence, the detrimental effects on the mould will be more serious.

4.2.6. Effect of cyclic loading on the mould

In practice, there is always more than one production cycle on the mould. The residual stress and distortion accumulate with the cyclic loading. The evolutions of axial residual

displacement and Mises stress at critical nodes within five production cycles are shown in Figs. 16 and 17.

The residual Mises stress seems unlikely to provoke any crack directly in the initial usage of the mould, as it remains lower than the 0.2% yield strength of the materials at room temperature. However, it does increase with the loading cycles. Although the increase of the residual values is somewhat slow, it may accumulate up to a certain critical value after many loading cycles and come close to the true elastic limit of 100 MPa. It is, nevertheless, obvious that at temperatures higher than 500 °C, stresses overcome the elastic limits. To take into account this phenomenon, work will be continued taking into account a more complex unified cyclic elasto-visco plastic behavior model.

Table 4
Comparison of critical items for different forming times

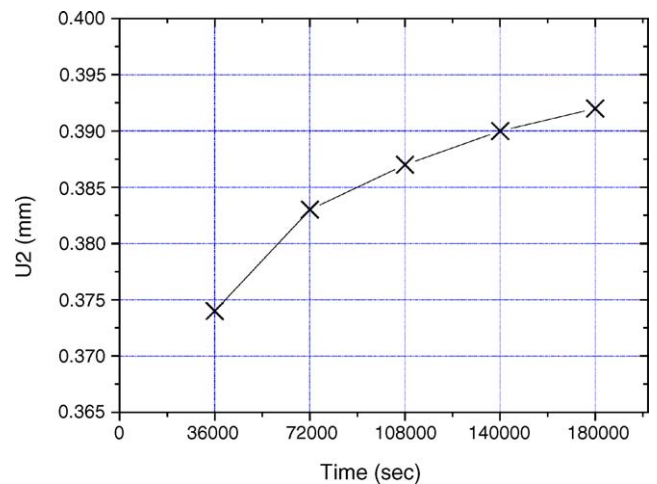| Items	Forming time (h)		
	1	10	20
U1_max (mm)	2.901E−2	3.645E−2	3.866E−2
U2_max (mm)	3.516E−1	3.740E−1	4.012E−1
Mises_max (MPa)	8.244E+1	9.378E+1	9.647E+1

Fig. 16. Evolution of axial residual displacement U2 at N2281 within five cycles.
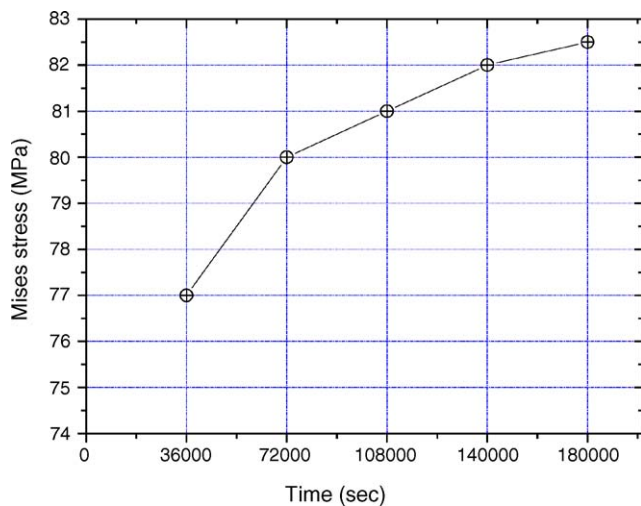
Fig. 17. Evolution of residual Mises stress at N3540 within five cycles.

5. Conclusion

The effects of residual stress and distortion on the refractory steel tools used for superplastic forming were investigated by a thermomechanical stress analysis using an axisymmetric model. Submitted to a whole industrial forming step, the following results can be pointed out:

- a low thermal gradient in the mould is sufficient to cause geometrical distortion, and induce high stresses after the application of the clamping load ensuring the tightness of the mould for gas introduction;
- stresses induced by the forming load can be neglected when compared to those coming from clamping loads. Moreover, they are not concentrated at the same locations of the mould. As a consequence, simulation of sheet forming can be omitted when the interest of calculation focuses on mould damage;
- during the sheet forming period, the refractory steel mould is subjected to creep, most of the stress is relaxed within less than 600 s and creep strain are generated mainly in the central region of the mould;
- after the cooling period, a residual geometrical distortion of the mould is predicted. This distortion increases with the production cycles, and can impair the dimension precision of the produced components;
- even if the level of stresses estimated in the simulation cannot explain damages of moulds, other elements have to be considered in the future, like an increase of the thermal gradient during heating and cooling period, or local thermal gradient on the surfaces during the sheet removal period.

Work is in progress to investigate both numerically and experimentally the crack propagation in SPF moulds. This will be greatly beneficial to understand processes of tool damage, namely by relating the behavior of dies to both microstructural and thermomechanical features.

References

[1] M.T. Cope, N. Ridley, Superplastic deformation characteristics of micro-duplex Ti–6Al–4V alloy, Mater. Sci. Technol. 2 (1986) 140–145.
[2] V. Vasquez, T. Altan, New concepts in die design-physical and computer modeling applications, J. Mater. Process. Technol. 98 (2) (2000) 212–223.
[3] S.I. Oh, W.T. Wu, K. Arimoto, Recent developments in process simulation for bulk forming processes, J. Mater. Process. Technol. 111 (1–3) (2001) 2–9.
[4] D. Sanders, Reinforced ceramic dies for superplastic forming operations, in: G. Bernhart, T. Cutard, P. Lours (Eds.), The Third European Conference on Superplastic Forming, EuroSPF04, Ecole des Mines d'Albi-Carmaux, Albi, France, July, 2004, pp. 109–115.
[5] A.J. Bames, Industrial application of superplastic forming: trends and prospects, Mater. Sci. Forum 357–359 (2001) 3–16.
[6] V. Garat, G. Bernhart, L. Hervy, Influence of design and process parameters on service life of nut hot forging dies, J. Mater. Process. Technol. 147 (2004) 359–369.
[7] P. Lours, S. Baleix, G. Bernhart, in: T. Chandra, K. Higashi, C. Suryanarayana, C. Tome (Eds.), Investigation on the Damage of Superplastic Forming Tools, Elsevier Science, UK, 2001, J. Mater. Process. Technol. (CDROM Special Issue).
[8] S. Baleix, Y. Le Maoult, S. Frenois, Y. Marcel, P. Lours, G. Bernhart, Simulation of service life cycle induced thermomechanical stresses in a superplastic forming tool, in: Proceedings of the Third International Congress on Thermal Stresses, Cracow, Poland, 3 July, 1999.
[9] S. Baleix, G. Bernhart, P. Lours, Oxidation and oxide spallation of heat resistant cast steels for superplastic forming dies, Mater. Sci. Eng. A 327 (2) (2002) 155–166.
[10] S. Baleix, S. Le Roux, G. Bernhart, P. Lours, Surface and image analysis of oxides grown and spalled on heat resistant cast steels exposed to thermal cycles, J. Mater. Process. Technol. 118 (1–3) (2001) 321–328.
[11] P. Lours, T. Cutard, G. Bernhart, C. Levaillant, Performance of metallic and ceramic tools for superplastic forming, Int. J. Mater. Prod. Technol., SPM1 vol. 2 (2001) 445.
[12] D. Recorbet, Creep Properties of Refractory Steels, Report S-97/4283000F2, DGA-CEAT, 2001.
[13] P. Lours, S. Baleix, G. Bernhart, First Annual Research Report on SPF dies, Report SPF/RAI/06/98, ENSTIMAC, 1998.
[14] Y.H. Kim, S.S. Hong, J.S. Lee, R.H. Wagoner, Analysis of superplastic forming processes using a finite-element method, J. Mater. Process. Technol. 62 (1996) 90–99.
[15] J.-L. Chenot, L. Fourment, K. Mocellin, Numerical treatment of contact and friction in FE simulation of forming processes, J. Mater. Process. Technol. 125–126 (2002) 45–52.
[16] S. Baleix, P. Lours, G. Bernhart, High Temperature Mechanical Behavior of Ni–Cr–Fe Heat Resistant Cast Steel, ICM8, Victoria, Canada, May 16–21, 1999.